Geophysical Research Letters

RESEARCH LETTER
10.1029/2019GL086230

Logarithmic Growth of Dikes From a Depressurizing Magma Chamber

Benjamin E. Grossman-Ponemon[1], Elías R. Heimisson[2,3], Adrian J. Lew[1,4], and Paul Segall[2]

[1]Department of Mechanical Engineering, Stanford University, Stanford, CA, USA, [2]Department of Geophysics, Stanford University, Stanford, CA, USA, [3]Now at Seismological Laboratory, California Institute of Technology, Pasadena, CA, USA, [4]Institute for Computational and Mathematical Engineering, Stanford University, Stanford, CA, USA

Key Points:
- Fully coupled simulations of dike growth and magma chamber depressurization are performed
- A simple model for dike length with time is identified and compared to seismic observations
- A simple model of chamber pressure versus dike length is derived and compared to simulations

Supporting Information:
- Supporting Information S1

Correspondence to:
B. E. Grossman-Ponemon and E. R. Heimisson,
bponemon@stanford.edu;
eliasrh@stanford.edu

Citation:
Grossman-Ponemon, B. E., Heimisson, E. R., Lew, A. J., & Segall, P. (2020). Logarithmic growth of dikes from a depressurizing magma chamber. *Geophysical Research Letters*, *47*, e2019GL086230. https://doi.org/10.1029/2019GL086230

Received 12 NOV 2019
Accepted 4 FEB 2020
Accepted article online 10 FEB 2020

Abstract Dike propagation is an intrinsically multiphase problem, where deformation and fluid flow are intricately coupled in a fracture process. Here we perform the first fully coupled simulations of dike propagation in two dimensions, accounting for depressurization of a circular magma chamber, dynamic fluid flow, fracture formation, and elastic deformation. Despite the complexity of the governing equations, we observe that the lengthening is well explained by a simple model $a(t) = c_1 \log(1 + t/c_2)$, where a is the dike length, t is time, and c_1 and c_2 are constants. We compare the model to seismic data from eight dikes in Iceland and Ethiopia, and, in spite of the assumption of plane strain, we find good agreement between the data and the model. In addition, we derive an approximate model for the depressurization of the chamber with the dike length. These models may help forecast the growth of lateral dikes and magma chamber depressurization.

Plain Language Summary Volcanic dike intrusions, propagating magma-filled fractures, precede most eruptions. Dike propagation has been studied for decades through simplified analytical and numerical models. To date, no study has fully addressed how the fluid magma, host rock, and the magma chamber all interact at the same time and drive the dike forward. We present such simulations for a two-dimensional configuration and deduce that a simple formula can explain how the dike lengthens with time. We suggest that this simple formula may be used to forecast dike growth.

1. Introduction

Modeling of dike propagation has remained a topic of active research to this day since the seminal work of Anderson (1937, 1951), yet many modeling challenges remain unsolved (Rivalta et al., 2015). One is computationally and theoretically rigorous modeling of the fully coupled system, which includes fluid flow, host rock deformation, fracture formation, and depressurization of a magma chamber. Many studies that couple fluid flow and elastic deformation make the simplifying approximation that dike opening is proportional to the local fluid pressure (Pinel & Jaupart, 2000; Pinel et al., 2017), which is not generally valid. Other studies have treated fluid flow and elastic coupling more rigorously for straight dikes (e.g., Lister & Kerr, 1991;Rubin, 1995). However, these studies have not explored the coupling of the dike to the magma chamber through mass exchange and elastic stress transfer. As a result, the space-time behavior of laterally propagating dikes and their coupling to a magma chamber are not fully understood. Laterally propagating dikes are the most commonly observed in field studies (Townsend et al., 2017), and thus, understanding their dynamics and emplacement is of great importance to the interpretation of field observations as well as to volcano monitoring and hazard mitigation. New oceanic crust on Earth, and perhaps other planets, is primarily generated by dike injections (Wright et al., 2012). Thus, dike dynamics play an important role in the evolution of the crust and lithosphere on a global scale. As the mathematical model of dike propagation from a magma chamber resembles the early time growth of a hydraulic fracture from a pressurized wellbore, similar problems have been of interest in the hydraulic fracturing community (e.g., Bunger et al., 2010; Detournay & Carbonell, 1997; Garagash & Detournay, 1997).

Dike propagation is typically associated with migrating seismic swarms. The advancing front of the swarm coincides approximately with the dike tip location (section 3.3). Thus, the migration speed of the seismic swarm represents the dike propagation speed, and earthquake epicenters delineate the dike path and length

(e.g., Sigmundsson et al., 2015). Persistent normal faulting above the dike may accompany the intrusion (Belachew et al., 2012), which does not necessarily map the dike tip. As a crustal dike grows it removes magma from the magma chamber, thereby dropping the chamber pressure and decreasing the chamber volume. The volume change can often be inferred from geodetic measurements.

Our contribution to this problem is twofold. First, we apply a finite element-based method (Grossman-Ponemon & Lew, 2019) to simulate the fully coupled hydraulic fracture problem in two dimensions. Although the method can be used to simulate curvilinear trajectories, for simplicity we restrict our attention to straight propagation. Straight dike propagation is usually appropriate for rift zone volcanism such as in Iceland, Ethiopia, and Hawaii. Second, we use the simulation results as a guide to establish simplified expressions relating the chamber pressure in and dike length, and the dike length and time. These simplified models provide insight into the important mechanisms driving the evolution of the problem.

2. Mathematical Model

We model a magma chamber as a circular cavity of radius R and time-varying pressure $P_v(t)$ (see Figure 1). We assume plane strain deformation and an infinite, isotropic, linear elastic rock with shear modulus μ, Poisson's ratio ν, and fracture toughness K_{Ic}. The storage of magma in the chamber is characterized by the constant $\beta := \rho_m^{-1}\mathrm{d}\rho_m/\mathrm{d}P_v + V_c^{-1}\mathrm{d}V_c/\mathrm{d}P_v$, where $\rho_m(P_v)$ and $V_c(P_v)$ are the (assumed spatially uniform) magma density in the chamber and the chamber volume, respectively (Rivalta, 2010). We call β the total compressibility. The rock is loaded in the far field via in situ stresses. We align the x and y axes with the principal stresses S_x and S_y, respectively, and we assume $S_x \geq S_y$ (with compression positive). Opening against the minimum stress is a dike of length $a(t)$, partially filled to length $\ell(t)$ by magma. The dike propagates quasi-statically. Within the dike, we model the flow of magma with Reynolds lubrication theory, treating it as an incompressible, laminar, Newtonian fluid with viscosity η. Thus, the compressibility of the magma is accounted for inside the chamber, but not within the dike. In the unimpinged or unwetted portion of the dike, which we call the dike tip cavity, we assume that the exsolved gases and fluids from the magma and host rock produce a pressure $P_t \leq P_v(t)$ (cf. Rubin, 1993b).

The governing equations of the above system are similar to those of linear elastic, hydraulic fracturing problems in the literature (e.g., Detournay, 2016; Garagash, 2006). Changes to the boundary conditions arise due to the coupling between the dike and the magma chamber (see supporting information).

We subtract the mean stress $M = (S_x + S_y)/2$ without altering the problem (cf. Mériaux & Lister, 2002). The resulting chamber overpressure is $p_v(t) = P_v(t) - M$, the tip underpressure is $p_t = P_t - M$, and the rock is loaded by the far-field stress deviator $S = (S_x - S_y)/2$. Henceforth, we will term these quantities chamber pressure, tip pressure, and deviatoric stress, respectively. We introduce the following characteristic length (a_c), stress/pressure (p_c), displacement/dike aperture (w_c), and time (t_c):

$$a_c = R, \quad p_c = S, \quad w_c = \frac{RS}{\mu}, \quad t_c = \frac{\eta\mu^2}{S^3}, \tag{1}$$

where t_c represents a characteristic timescale for magma flow within the dike. If the chamber radius is of order 1 km, the magma viscosity 100 Pa s (Wada, 1994), the shear modulus 10 GPa, and deviatoric stress 1 MPa (Jónsson, 2012), then the characteristic aperture and time are $w_c = 0.1$ m and $t_c = 10,\ 000$ s, respectively. The latter, being approximately 3 hr, is reasonable given observed duration of diking events. We normalize all relevant quantities by these characteristic dimensions. To differentiate the nondimensionalized quantities, we use the tilde symbol (e.g., $\tilde{p}$ versus p).

When we nondimensionalize the problem using (1), four dimensionless parameters arise in the governing equations in addition to Poisson's ratio ν. These are related to the toughness of the rock, the compressibility, the tip pressure, and the initial chamber pressure. Respectively, we denote these

$$\mathcal{K} = \frac{K_{Ic}}{SR^{1/2}}, \quad \mathcal{B} = \beta\mu, \quad \mathcal{T} = \frac{p_t}{S}, \quad \mathcal{P} = \frac{p_v(0)}{S}. \tag{2}$$

By our choice of t_c, the viscosity of the magma drops out of the governing equations. Additionally, the ratio $\tilde{a} = a/R$ is important in the elasticity kernels, behaving similarly to the length versus depth parameter of a near-surface hydraulic fracture (Zhang et al., 2005).

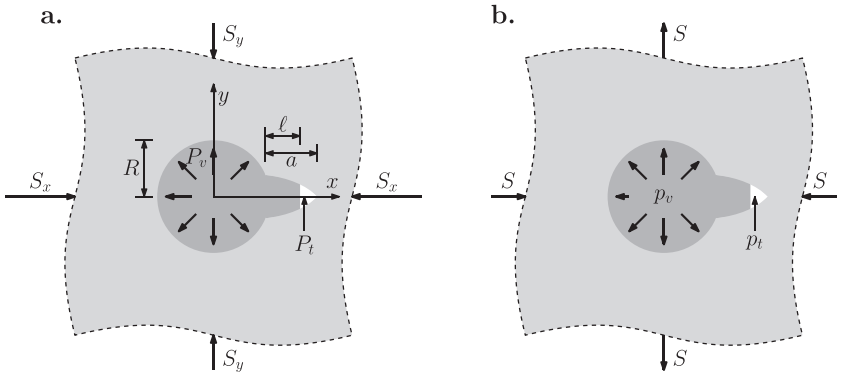

Figure 1. (a) Plan form view of the radial dike problem, with relevant dimensions and pressures labeled (see text). (b) Problem with mean stress $M = (S_x+S_y)/2$ subtracted. In both figures, the dike is depicted with exaggerated opening.

For a circular hole, $V_c^{-1}\mathrm{d}V_c/\mathrm{d}P_v = 1/\mu$, and hence $\mathcal{B} = \mu\beta \geq 1$. The case $\mathcal{B} = 1$ corresponds to incompressible magma (i.e., $\rho_m^{-1}\mathrm{d}\rho_m/\mathrm{d}P_v = 0$). Meanwhile, we generally expect the parameter $\mathcal{T}$ to fall in the range $[-M/S, -1]$. If a vacuum exists in the dike tip cavity, then $\mathcal{T} = -M/S$. The case $\mathcal{T} = -1$ corresponds to the tip pressure equilibrating with the deviatoric stress (equivalently, the net pressure in the dike tip cavity P_t equals the minimum in situ stress $S_y = M - S$). If the tip pressure were larger, the dike would grow unstably (see supporting information).

There is uncertainty in the appropriate values for fracture toughness, with laboratory measurements between roughly 0.1 and 10 MPa $\mathrm{m}^{1/2}$ (Atkinson & Meredith, 1987). However, field studies of dike process zones suggest the fracture toughness may be 2 or 3 orders of magnitude larger (Delaney et al., 1986), suggesting that a value of 100 MPa $\mathrm{m}^{1/2}$ maybe more likely (see Townsend et al., 2017). Based on previous estimates for the chamber radius and deviatoric stress, we expect $\mathcal{K}$ between 0.003 and 3, with the larger value corresponding to estimates based on dike process zones.

Based on the scale of dikes observed in nature, we are interested in parameter combinations for which $\tilde{a}$ is approximately between 10^{-1} and 10^{1}, where we believe our model to be most applicable (i.e., dikes with length between 100 m and 10 km for a chamber radius of order 1 km). For smaller lengths, thermal and viscous effects, and preexisting cracks are necessary to study how dikes nucleate. When the dike is long and propagation speed becomes small then solidification of the magma becomes important due to decreased flow rate (Rubin, 1993a).

3. Simulation Results and Simplified Models

Next, we describe the results of the fully coupled simulations. In analyzing the results, we explored simple relations that can explain the observed time dependence of the system.

Within the $\{\mathcal{K}, \mathcal{B}, \mathcal{P}, \mathcal{T}\}$-parameter space, we investigated the behavior of the system under $\mathcal{K} = 3$, the upper end of our expected range, and varying $\mathcal{B} \in \{1, 2, 4, 8, \infty\}$ and $\mathcal{P} \in \{2.5, 5, 10, 20\}$. We selected $\mathcal{T} = -\mathcal{P}$ (i.e., $p_t = -p_v(0)$). One such situation where this occurs is if the tip cavity pressure is 0 ($P_t = 0$), while the initial chamber pressure doubles the mean stress ($P_v(0) = 2M$), in which case $\mathcal{T} = -\mathcal{P} = -M$. Poisson's ratio was $\nu = 0.25$.

We chose the scaling of $\{\mathcal{K}, \mathcal{P}, \mathcal{T}\}$ for three reasons (see also supporting information). First, for a given initial dike to be critical ($K_I = K_{Ic}$), increasing $\mathcal{P}$ meant either increasing $\mathcal{K}$ or decreasing $\mathcal{T}$ to balance the increased chamber pressure, and we opted for the latter. Second, for our choice of $\mathcal{K}$, if $\mathcal{T}$ is significantly greater than $-\mathcal{P}$, dikes could become supercritical ($K_I > K_{Ic}$) at early times, implying the crack tip would propagate at speeds comparable to seismic wave speeds. This is unlikely to occur in nature since dike-induced seismic swarms propagate at much lower speed (cf. section 3.3). Lastly, for $\mathcal{T}$ significantly less than $-\mathcal{P}$, the initial dike tip cavity becomes very small with respect to the dike length. Resolving the dike tip cavity at early times is computationally prohibitive.

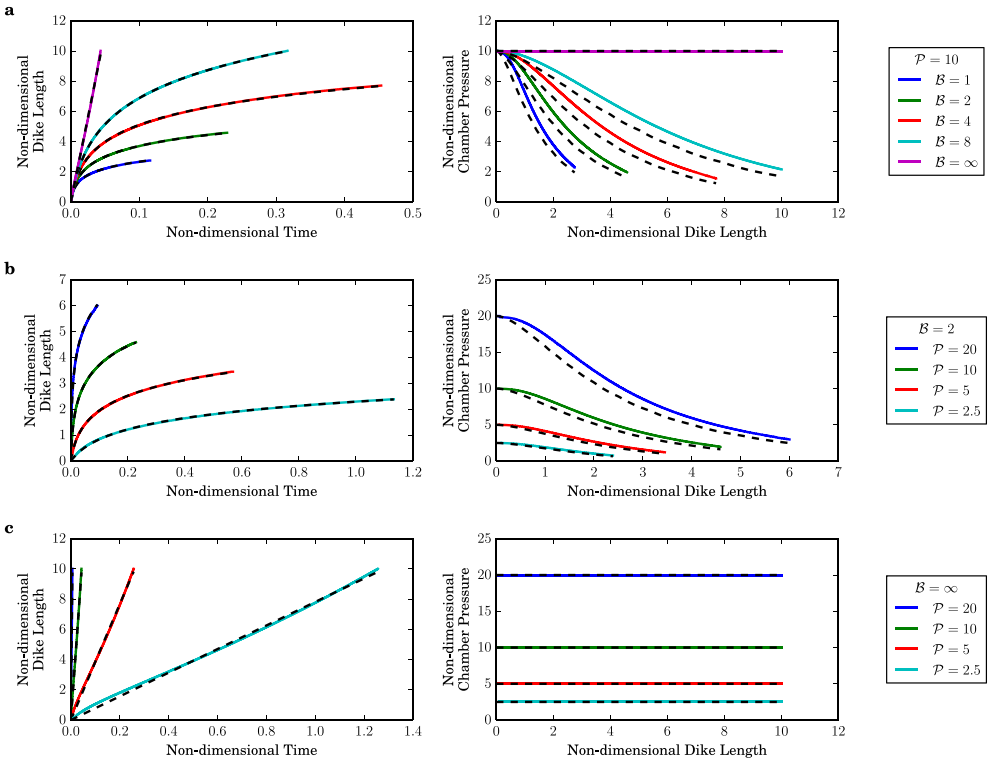

Figure 2. Dike length versus time and chamber pressure versus dike length for (a) $\mathcal{P} = 10$ and varying $\mathcal{B}$, (b) $\mathcal{B} = 2$ and varying $\mathcal{P}$, and (c) $\mathcal{B} = \infty$ and varying $\mathcal{P}$. The fitted model for dike length versus time equation (3) and the simplified pressure versus dike length model equation (5) are shown with black dashed lines.

In the supporting information, we explored the effect of increasing and decreasing $\mathcal{T}$ while keeping the other parameters fixed, and we found that, as long as the dike did not become supercritical, the behavior was largely unaffected by the choice of tip pressure.

The simulations were terminated under one of two conditions: either the dike became too large with respect to the computational domain, or the lag $(a(t) - l(t))$ became equal to the minimum mesh size. For further details of the simulations see the supporting information. In Figure 2, we show the length of the dike versus time and the pressure in the magma chamber versus dike length for fixed $\mathcal{P} = 10$ and varied $\mathcal{B}$, fixed $\mathcal{B} = 2$ and varied $\mathcal{P}$, and fixed $\mathcal{B} = \infty$ and varied $\mathcal{P}$. The other cases are shown in the supporting information.

3.1. Dike Growth Versus Time

In all cases, the dike length history could be closely represented by the simple relation (cf. dashed curves in Figure 2)

$$\tilde{a}_{\text{model}}(\tilde{t}) = \dot{a}^* t^* \log(1 + \tilde{t}/t^*), \tag{3}$$

where $\dot{a}^*$ and t^* represent characteristic growth rate and timescale respectively, which we determined by least squares fitting of the simulated growth. We contrast equation (3) with (Rivalta, 2010), where an exponential decay of dike velocity based on a quasi-static mass balance between a dike and a chamber was derived. We found exponential decay to be inconsistent with the fully coupled simulations. Equation (3) can be expressed in terms of a characteristic length $a^* = \dot{a}^* t^*$; however, the above definition is favorable because in the limit $t^* \to \infty$, $\tilde{a}_{\text{model}}(\tilde{t}) \to \dot{a}^* \tilde{t}$. This limiting case arises when the magma chamber does not depressurize (i.e., $\mathcal{B} \to \infty$, shown in Figure 2c) and is explored later. The model above assumes growth starting at $\tilde{t} = 0$. If the dike is initially subcritical then we may shift time by some $\tilde{t}_{\text{start}} > 0$ (see supporting information for details).

The agreement between equation (3) and the simulations is remarkable. In over half of the parameter combinations explored, this simple model could explain more than 99.9% of the variance in the simulated trajectories based on computing an $R^2 = 1 - \chi_{\text{res}}/\chi_{\text{tot}}$ value. The term $\chi_{\text{res}} = \sum_{i=1}^{N} (\tilde{a}(t_i) - \tilde{a}_{\text{model}}(t_i))^2$ is the

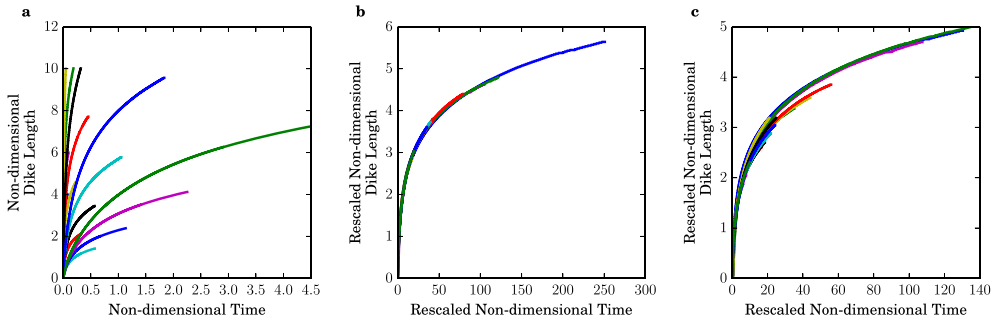

Figure 3. Dike length versus time for all simulations with $\mathcal{B} < \infty$: (a) original data, with length and time normalized as in (1), (b) length and time data rescaled by the least squares fit for a^* and t^* for each simulation, and (c) length and time data rescaled by the unified fit (4). When rescaled the curves collapse in both cases.

sum of squares of the residuals between simulations and equation (3), respectively, at each of the N time steps. Similarly, $\chi_{\text{tot}} = \sum_{i=1}^{N} (\tilde{a}(t_i) - \overline{\tilde{a}})^2$ is the sum of squares of the residuals between simulations and their mean value. All fits had a variance reduction greater than 99.3%. Furthermore, all 20 simulations could be fit simultaneously with a variance reduction of 99.4% using

$$\dot{a}^* \approx 0.66\mathcal{P}^{2.57^{+0.10}_{-0.14}} \qquad a^* = \dot{a}^* t^* \approx 0.82\mathcal{B}^{0.65^{+0.07}_{-0.07}} \qquad t^* = a^*/\dot{a}^*, \tag{4}$$

where we provided 95% confidence window for the exponents. The confidence bounds were determined by resampling the entire simulation time series with replacement for a set of all 20 simulations and estimating the exponents. The uncertainty thus reflects the range of values that may be found if only a subsample of the simulations were available. Exponents $\mathcal{P}^{2.57}$ and $\mathcal{B}^{0.65}$ corresponded to fitting all available simulations. Equation (4) provides insight into how the characteristic time, speed and length vary as compressibility and/or pressure change.

In Figure 3a, we show $\tilde{a}$ versus $\tilde{t}$ for each of the simulations with $\mathcal{B} < \infty$. We then show that the curves collapse when we rescale the simulated dike length and time by the least squares fits for a^* and t^* for each simulation and by using the unified fit of equation (4) in Figures 3b and 3c, respectively.

3.2. Chamber Pressure Versus Dike Length

To better understand the chamber pressure versus dike length (Figure 2, right column), we consider a simplified model based on three assumptions. We neglect the length of the dike tip cavity (i.e., we take $\ell = a$), we assume the magma pressure is uniform throughout the dike and equal to p_v, and we assume the initial dike length is very small compared to the chamber radius. Under these assumptions, we find (cf. the supporting information)

$$\tilde{p}_{v,\text{model}}(\tilde{a}) = \frac{\pi\mathcal{B}\mathcal{P} - \tilde{v}_S(\tilde{a})}{\pi\mathcal{B} + \tilde{v}_p(\tilde{a})}, \tag{5}$$

where $\tilde{v}_p(\tilde{a})$ and $\tilde{v}_S(\tilde{a})$ denote the nondimensional crack volume (defined $\tilde{v} = \mu V/R^2$) associated with unit magma pressure and deviatoric stress, respectively. These functions may be computed from the solution of (Tweed & Rooke, 1973). No closed-form expressions exist for the functions $\tilde{v}_p(\tilde{a})$ and $\tilde{v}_S(\tilde{a})$, plotted in Figure 4. However, they are well approximated by

$$\tilde{v}_p(\tilde{a}) \approx \tilde{a}^2 \frac{2.96 + \frac{3\pi}{16}\left(\frac{\tilde{a}}{0.636}\right)^{0.915}}{1 + \left(\frac{\tilde{a}}{0.636}\right)^{0.915}} \qquad \tilde{v}_S(\tilde{a}) \approx \tilde{a}^2 \frac{5.92 + \frac{3\pi}{16}\left(\frac{\tilde{a}}{0.369}\right)^{1.03}}{1 + \left(\frac{\tilde{a}}{0.369}\right)^{1.03}} \tag{6}$$

as shown by the black dashed lines in the same figure.

The validity of equation (5) could be tested by using geodetic measurements as a proxy for pressure and migration of seismicity as a proxy for dike length. We leave for future research to identify the appropriate data sets and methodology to make this comparison.

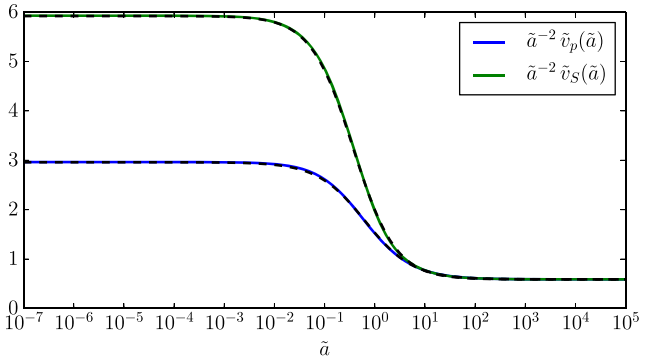

Figure 4. Nondimensional crack volume functions for a circular hole with a straight edge crack subjected to unit far-field hydrostatic tension (blue curve) and deviatoric stress (green curve), computed using the elasticity solution of Tweed and Rooke (1973). Black dashed lines correspond to the approximations (6). For $\tilde{a} < 10^{-2}$ and $\tilde{a} > 10^{1}$, the elasticity behavior is well approximated by an edge crack and an internal crack with no magma chamber, respectively.

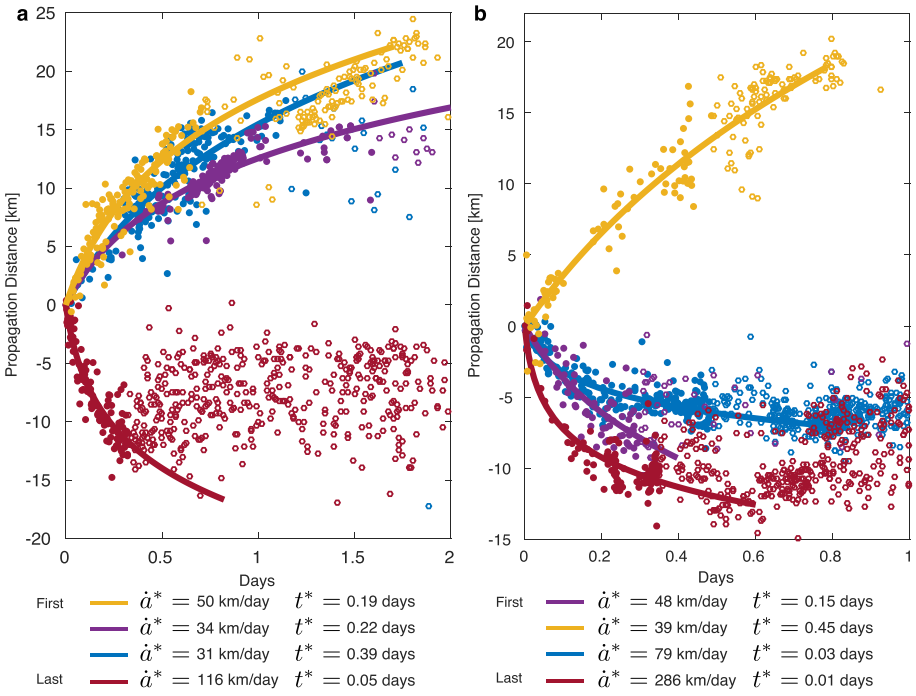

Figure 5. Comparison of equation (3) to four diking events in Afar, Ethiopia (a) and Krafla, Iceland (b). Lines are fits of equation (3) to the seismicity (filled circles). Hollow circles are later seismicity and are not fitted. The lines tend to envelope the hollow circles, suggesting that the model may predict that growth of the dike. In a, blue = July 2008, purple = March 2008, red = October 2008, yellow = November 2007 dikes (Belachew et al., 2011; Tepp et al., 2016). In b, blue = February 1980, purple = September 1977, red = March 1980, yellow = July 1978 dikes (Brandsdóttir & Einarsson, 1979; Einarsson & Brandsdóttir, 1980). The quantities $\dot{a}^*$ and t^* are reported with dimensions; precise values of the physical parameters needed to nondimensionalize using a_c and t_c are not known.

For simulations with $\mathcal{B} < \infty$, the model consistently under-fit the pressure, due to the overestimate of the magma volume in the dike via neglect of the tip effects. The maximum point-wise discrepancy $\max_{i=1,\ldots,N} \left|\tilde{p}_v(\tilde{a}_i) - \tilde{p}_{v,\text{model}}(\tilde{a}_i)\right|$ varied between 6.4% and 11.8% of the initial value $\tilde{p}_v(0)$. The agreement between the model and the full system is remarkable and consistent with the tip region contributing little to the overall mass in the dike. In the supporting information, we present and analyze a second model that accounts for the tip effects.

3.3. Comparison to Seismicity

A propagating dike typically triggers a propagating swarm of seismicity near the dike tip, which can be inferred from joint interpretation of seismic and geodetic data (Heimisson & Segall, 2020; Sigmundsson et al., 2015). Particularly strong evidence for this relationship was established when the seismic swarm of the September 1977 Krafla dike (purple, Figure 5b) reached the location of a geothermal borehole (Brandsdóttir & Einarsson, 1979) and a small eruption was produced from the borehole (Larsen & Grönvold, 1979), thus directly demonstrating the collocation of the advancing seismicity and magma.

The agreement between equation (3) and the simulations in Figure 2 suggests that this simple functional form for how dikes grow may be robust and relatively invariant of the details of the system. In order to test this hypothesis, we compared equation (3) to the time evolution of swarms of seismicity triggered by propagating dikes (Figure 5). We observe agreement between the log model and the seismicity data in Figure 5, which provides observational support for equation (3). The fitting in Figure 5 used only a part of the earthquake locations (filled circles). However, the model still followed the advancement of later events (hollow circles), thus indicating potential forecasting capabilities. We suggest that (3) and (5) could be used together or separately to forecast the time evolution of dike propagation and chamber depressurization.

To make the comparison in Figure 5 between equation (3) to the propagating seismicity recorded during diking events in Iceland and Ethiopia we collected catalogs from the Dabbahu-Manda Hararo rift in Afar, Ethiopia (Belachew et al., 2011; Tepp et al., 2016) and the Krafla rifting episode, Iceland (Brandsdóttir &

Einarsson, 1979; Einarsson & Brandsdóttir, 1980). We limited attention to large dikes that showed clear migration of seismicity with time, which resulted in four dikes from each rifting episode being selected for the analysis. Each event was projected onto the nearest point on a line fit through the entire swarm. We then computed the distance from the average location of the first events. We selected one to five events to determine this location, depending on the number of recorded events at the initial stages of the swarm before clear signs of migration occur. We fit (3) to the migration distance of the filled symbols in Figure 5. The fitting was done by minimizing an L_1 norm in order to decrease the influence of outliers.

4. Discussion

We performed fully coupled simulations of a dike propagating laterally away from a magma chamber in two dimensions that resolves the coupling of fluid and solid phases. We identified a simple relationship that indicates that dikes grow approximately with the logarithm of time (3). Further, we attain a simple relationship for how pressure in the magma chamber decreases with the length of the dike (5).

We leave for future research a derivation of (3) or a comparable relationship. Our analysis suggests that the logarithmic growth is a manifestation of an intermediate dike length behavior and cannot be explained by the expected dynamics for very small ($\tilde{a} \ll 1$) or large ($\tilde{a} \gg 1$) dikes compared to the chamber radius. This is evidenced by the nondimensional crack volumes shown in Figure 4. When $\tilde{a} < 10^{-2}$ and $\tilde{a} > 10^{1}$, the crack behaves as an edge crack or an internal crack with no magma chamber, respectively.

Remarkably, the logarithmic growth model, inspired by two-dimensional behavior, agrees with three-dimensional seismic observations. We suggest that this result can be used to forecast dike growth and the accompanied depressurization and may provide a new way to jointly interpret seismic and geodetic observations. Moreover, we have presented a methodology that couples numerical simulations and analytical analysis in a unique way. Our methodology provides new insights into a physically complicated system evolving in a transitory regime.

Acknowledgments
E. R. H. was supported by NASA under the NESSF Program—Grant NNX16AO40H. P. S. and E. R. H were supported by NASA ROSES ESI—Grant NNX16AN08G. A. J. L. and B. E. G. P. were supported by NSFCMMI-1662452. B. E. G. P. and E. R. H. contributed equally to this work. E. R. H. was responsible for running simulations, and B. E. G. P. for code development and implementing the numerical approach. We thank Cynthia Ebinger and an anonymous reviewer for their constructive remarks. All data in this study are shown in Figure 5 and are found in Belachew et al. (2011), Brandsdóttir and Einarsson (1979), Einarsson and Brandsdóttir (1980), and Tepp et al. (2016).

References

Anderson, E. M. (1937). IX.—The dynamics of the formation of cone-sheets, ring-dykes, and caldron-subsidences. *Proceedings of the Royal Society of Edinburgh*, *56*, 128–157. https://doi.org/10.1017/S0370164600014954

Anderson, E. M. (1951). *The dynamics of faulting and dyke formation with applications to Britain*. New York: Hafner Pub. Co.

Atkinson, B. K., & Meredith, P. G. (1987). Experimental fracture mechanics data for rocks and minerals. In B. K. Atkinson (Ed.), *Fracture mechanics of rock* (pp. 477–525). London: Academic Press.

Belachew, M., Ebinger, C., Coté, D, Keir, D., Rowland, J., Hammond, J. O., & Ayele, A. (2011). Comparison of dike intrusions in an incipient seafloor-spreading segment in Afar, Ethiopia: Seismicity perspectives. *Journal of Geophysical Research*, *116*, B06405. https://doi.org/10.1029/2010JB007908

Belachew, M., Ebinger, C., & Coté, D. (2012). Source mechanisms of dike-induced earthquakes in the Dabbahu-Manda Hararo rift segment in Afar, Ethiopia: Implications for faulting above dikes. *Geophysical Journal International*, *192*(3), 907–917. https://doi.org/10.1093/gji/ggs076

Brandsdóttir, B., & Einarsson, P. (1979). Seismic activity associated with the September 1977 deflation of the Krafla central volcano in northeastern Iceland. *Journal of Volcanology and Geothermal Research*, *6*(3-4), 197–212. https://doi.org/10.1016/0377-0273(79)90001-5

Bunger, A. P., Lakirouhani, A., & Detournay, E. (2010). Modelling the effect of injection system compressibility and viscous fluid flow on hydraulic fracture breakdown pressure. In *Proceedings of the 5th Intern ational Symposium on In-Situ Rock Stress*, Beijing: International Society for Rock Mechanics and Rock Engineering.

Delaney, P. T., Pollard, D. D., Ziony, J. I., & McKee, E. H. (1986). Field relations between dikes and joints: Emplacement processes and paleostress analysis. *Journal of Geophysical Research*, *91*(B5), 4920–4938. https://doi.org/10.1029/JB091iB05p04920

Detournay, E. (2016). Mechanics of hydraulic fractures. *Annual Review of Fluid Mechanics*, *48*(1), 311–339. https://doi.org/10.1146/annurev-fluid-010814-014736

Detournay, E., & Carbonell, R. (1997). Fracture-mechanics analysis of the breakdown process in minifracture or leakoff test. *SPE production & facilities*, *12*(03), 195–199. https://doi.org/10.2118/28076-PA

Einarsson, P., & Brandsdóttir, B. (1980). Seismological evidence for lateral magma intrusion during the July 1978 deflation of the Krafla volcano in NE-Iceland. *Journal of Geophysics*, *47*(1), 160–165. Retrieved from https://journal.geophysicsjournal.com/JofG/article/view/134

Garagash, D. I. (2006). Propagation of a plane-strain hydraulic fracture with a fluid lag: Early-time solution. *International Journal of Solids and Structures*, *43*(18), 5811–5835. https://doi.org/10.1016/j.ijsolstr.2005.10.009

Garagash, D., & Detournay, E. (1997). An analysis of the influence of the pressurization rate on the borehole breakdown pressure. *International Journal of Solids and Structures*, *34*(24), 3099–3118. https://doi.org/10.1016/S0020-7683(96)00174-6

Grossman-Ponemon, B. E., & Lew, A. J. (2019). An algorithm for the simulation of curvilinear plane-strain and axisymmetric hydraulic fractures with lag using the universal meshes. *International Journal for Numerical and Analytical Methods in Geomechanics*, *43*(6), 1251–1278. https://doi.org/10.1002/nag.2896

Heimisson, E. R., & Segall, P. (2020). Physically consistent modeling of dike induced deformation and seismicity: Application to the 2014 Bárðarbunga dike, Iceland. *Journal of Geophysical Research: Solid Earth*, *125*, e2019JB018141. https://doi.org/10.1029/2019JB018141

Jónsson, S. (2012). Tensile rock mass strength estimated using InSAR. *Geophysical Research Letters*, *39*, L21305. https://doi.org/10.1029/2012GL053309

Larsen, G., & Grönvold, K. (1979). Volcanic eruption through a geothermal borehole at Námafjall, Iceland. *Nature*, *278*, 707–710. https://doi.org/10.1038/278707a0

Lister, J. R., & Kerr, R. C. (1991). Fluid-mechanical models of crack propagation and their application to magma transport in dykes. *Journal of Geophysical Research*, *96*(B6), 10,049–10,077. https://doi.org/10.1029/91JB00600

Mériaux, C., & Lister, J. R. (2002). Calculation of dike trajectories from volcanic centers. *Journal of Geophysical Research*, *107*(B4), 2077. https://doi.org/10.1029/2001JB000436

Pinel, V., Carrara, A., Maccaferri, F., Rivalta, E., & Corbi, F. (2017). A two-step model for dynamical dike propagation in two dimensions: Application to the July 2001 Etna eruption. *Journal of Geophysical Research: Solid Earth*, *122*, 1107–1125. https://doi.org/10.1002/2016JB013630

Pinel, V., & Jaupart, C. (2000). The effect of edifice load on magma ascent beneath a volcano. *Philosophical Transactions of the Royal Society of London A: Mathematical, Physical and Engineering Sciences*, *358*(1770), 1515–1532. https://doi.org/10.1098/rsta.2000.0601

Rivalta, E. (2010). Evidence that coupling to magma chambers controls the volume history and velocity of laterally propagating intrusions. *Journal of Geophysical Research*, *115*, B07203. https://doi.org/10.1029/2009JB006922

Rivalta, E., Taisne, B., Bunger, A. P., & Katz, R. F. (2015). A review of mechanical models of dike propagation: Schools of thought, results and future directions. *Tectonophysics*, *638*, 1–42. https://doi.org/10.1016/j.tecto.2014.10.003

Rubin, A. M. (1993a). On the thermal viability of dikes leaving magma chambers. *Geophysical Research Letters*, *20*(4), 257–260. https://doi.org/10.1029/92GL02783

Rubin, A. M. (1993b). Tensile fracture of rock at high confining pressure: Implications for dike propagation. *Journal of Geophysical Research*, *98*(B9), 15,919–15,935. https://doi.org/10.1029/93JB01391

Rubin, A. M. (1995). Propagation of magma-filled cracks. *Annual Review of Earth and Planetary Sciences*, *23*(1), 287–336. https://doi.org/10.1146/annurev.ea.23.050195.001443

Sigmundsson, F., Hooper, A., Hreinsdottir, S., Vogfjörð, K., Ófeigsson, B. G., Heimisson, E. R., et al. (2015). Segmented lateral dyke growth in a rifting event at Bárðarbunga volcanic system, Iceland. *Nature*, *517*(7533), 191–195. Letter https://doi.org/10.1038/nature14111

Tepp, G., Ebinger, C. J., & Yun, S.-H. (2016). Spectral analysis of dike-induced earthquakes in Afar, Ethiopia. *Journal of Geophysical Research: Solid Earth*, *121*, 2560–2574. https://doi.org/10.1002/2015JB012658

Townsend, M. R., Pollard, D. D., & Smith, R. P. (2017). Mechanical models for dikes: A third school of thought. *Tectonophysics*, *703*, 98–118. https://doi.org/10.1016/j.tecto.2017.03.008

Tweed, J., & Rooke, D. P. (1973). The distribution of stress near the tip of a radial crack at the edge of a circular hole. *International Journal of Engineering Science*, *11*(11), 1185–1195. https://doi.org/10.1016/0020-7225(73)90084-0

Wada, Y. (1994). On the relationship between dike width and magma viscosity. *Journal of Geophysical Research*, *99*(B9), 17,743–17,755. https://doi.org/10.1029/94JB00929

Wright, T. J., Sigmundsson, F., Pagli, C., Belachew, M., Hamling, I. J., Brandsdóttir, B., et al. (2012). Geophysical constraints on the dynamics of spreading centres from rifting episodes on land. *Nature Geoscience*, *5*(4), 242. https://doi.org/10.1038/ngeo1428

Zhang, X., Jeffrey, R. G., & Detournay, E. (2005). Propagation of a hydraulic fracture parallel to a free surface. *International Journal for Numerical and Analytical Methods in Geomechanics*, *29*(13), 1317–1340.

Reference From the Supporting Information

Ágústsdóttir, T., Woods, J., Greenfield, T., Green, R. G., White, R. S., Winder, T., et al. (2016). Strike-slip faulting during the 2014 Bárdarbunga-Holuhraun dike intrusion, central Iceland. *Geophysical Research Letters*, *43*, 1495–1503. https://doi.org/10.1002/2015GL067423